Band Structures of Intercalation Compounds. The System $(NH_4)(NH_3)_3(TiS_2)_4$

Rafael Ramírez and Michael C. Böhm
Institut für Physikalische Chemie, Physikalische Chemie III, Technische Hochschule Darmstadt, Petersenstr. 20, D-6100 Darmstadt, West Germany

Z. Naturforsch. **42a**, 1346–1356 (1987); received August 17, 1987

Dedicated to Prof. Dr. K. G. Weil to the Occasion of his 60th Birthday

The electronic band structure of the intercalation system ammonia TiS_2 has been investigated by a semiempirical self-consistent-field (SCF) Hartree-Fock (HF) crystal orbital (CO) formalism supplemented by an INDO (intermediate neglect of differential overlap) Hamiltonian. A two-dimensional (2D) model for the title system with stoichiometry $(NH_4)(NH_3)_3(TiS_2)_4$ has been selected on the basis of available experimental data. The model is defined via a TiS_2 monolayer coupled to the intercalant monolayer. The corresponding band-structure properties are compared with band-structure calculations of monolayered TiS_2 and bulk TiS_2. For TiS_2 available experimental data and numerical results of conventional band-structure approaches are reported. The interaction between the guest-molecules and the host lattice has the character of a redox-process; i.e. one electron per formula unit has been transferred from the intercalant to the TiS_2 layer. One consequence of this transfer is a semiconductor-to-metal transition upon intercalation; an additional consequence is a remarkable electronic reorganization in the TiS_2 host. The surplus of electronic charge is predominantly localized at the S centers. The electronic states at the Fermi-level are of Ti 3d character. Two electronic configurations of the title system have been investigated. The mean-field ground state is of a charge density wave type with respect to the TiS_2 sublattice. A "symmetry adapted" (SA) configuration is predicted at higher energy.

1. Introduction

Transition-metal dichalcogenides form a class of compounds crystallizing in layered structures. Their physical properties are consequently strongly anisotropic [1, 2]. The common stoichiometry of these materials is TX_2. The transition-metal atoms T (T = Ti, Mo, Ta, Nb, Zr, etc.) and the chalcogenide atoms X (X = S, Se, Te) are arranged in a sandwich-like structure X .. T .. X. Each of the latter symbols stands for a two-dimensional (2D) network of closed-packed atoms. The 2D X .. T .. X layers of transition-metal dichalcogenides are coupled via weak van der Waals forces in the corresponding 3D solids (i.e. .. X X .. contacts). Various physical properties of these materials (i.e. transport numbers, mechanical, optical and electrical behaviour, superconductivity) are influenced by the 2D nature of the solids [1–3]. Phase transitions in combination with the formation of charge density waves (CDW) have been observed in a larger number of transition-metal dichalcogenides [4].

Reprint requests to Dr. M. C. Böhm, Institut für Physikalische Chemie, Physikalische Chemie III, Petersenstr. 20, D-6100 Darmstadt, West Germany.

One of the interesting properties of the above materials is their capability to intercalate guest atoms or molecules into the interlayer region [5]. The intrinsic properties of the host lattice TX_2 are often remarkably changed upon intercalation (e.g., generation of semiconductor-to-metal or metal-to-semiconductor transitions, changes in the superconducting transition temperature T_c, etc.) [3, 6].

Experimental investigations have shown that the atoms and molecules intercalated in transition-metal dichalcogenides are conventionally electron donors. The characterized intercalants can be divided into three larger groups [3, 5]: i) molecular systems of the Lewis-base type (i.e. amines, amides, pyridines, ammonia, hydrazine); ii) metal-atoms of the groups IA, IIA, IIB–VB; iii) transition-metal atoms of the 3d series. In earlier investigations it had been assumed that the intercalation of Lewis-base molecules in TX_2 host lattices allows for the conservation of the chemical composition of the guest molecules. More recent experimental work has shown that the formation of intercalation-systems is frequently accompanied by a redox-process. An example is the system "$NH_3 \cdot TiS_2$" where partial oxidation of the guest molecules has been observed [7]. This system contains in addition to

0932-0784 / 87 / 1100-1346 $ 01.30/0. – Please order a reprint rather than making your own copy.

NH_3 units also NH_4^+ ions leading to a final composition of $(NH_4^+)_y(NH_3)_{1-y}(TiS_2)^{y-}$. The value of y has been estimated by ^1H NMR spectroscopy and chemical analysis of derivatives where the NH_4^+ ions have been exchanged by alkaline atoms (ions). For TaS_2 and TiS_2 hosts $y = 0.1-0.2$ has been deduced [7, 8]. A comparable intercalation mechanism (i.e. redox-reaction between the host lattice and the guest) has been observed in the system pyridine TaS_2 [9].

Conductivity measurements are available for several intercalation systems. But to our knowledge no quantitative data have been reported for ammonia TiS_2. For the related hydrazine $TiSe_2$ system an increase of the room-temperature conductivity σ_{RT} by a factor of six upon intercalation has been observed. The temperature dependence of conductivity is metallic. At 10 K $\sigma \approx 10^5\,S\,cm^{-1}$ has been found, at 290 K $\sigma \approx 10^4\,S\,cm^{-1}$ [3].

The electronic band-structure properties of layered TX_2 materials have been reviewed by several authors [1, 10, 11]. Although the employed numerical tools differed in their quantitative results they allowed nevertheless for the evaluation of general trends in the corresponding band structures, i.e. the global character and sequence of the one-electron states. On the other side there is still a remarkable deficit in numerical investigations of the band structures of intercalated TX_2 materials. In the first place this is caused by the large unit-cell dimensions frequently encountered in the corresponding materials. The required computational expenditure is quite large. In addition to these technical boundaries conceptual problems are present; i.e. many intercalation-systems are not properly characterized from a structural and chemical point of view. One of the sparse available band-structure investigations concerns the system $LiTiS_2$. This solid has been investigated by a semiempirical non-self-consistent-field (SCF) tight-binding model [12] as well as by a semirelativistic linearized augmented-plane-wave (LAPW) approach [13]. An APW calculation of M_yTiS_2 (M = Fe, Cr) has been reported very recently [14].

It is the purpose of the present contribution to analyze the changes in the electronic structure of TiS_2 upon intercalation with ammonia, an intercalant of the Lewis-base type. We have employed a semiempirical SCF Hartree-Fock (HF) crystal orbital (CO) formalism based on an INDO (intermediate neglect of differential overlap) Hamiltonian. A detailed description of the 1 D variant of this CO formalism has been given in [15]. The theoretical background of the 2 D/3 D extension has been reported in [16]. For some recent applications of this band structure approach we refer to [17, 18] (1 D materials) and [19, 20] (2 D/3 D solids), respectively. The model Hamiltonian allows for the investigation of any atoms up to Br under the inclusion of the first transition-metal series.

The structural model adopted in the present investigation is defined via a TiS_2 monolayer supplemented by an additional monolayer of intercalated molecules. The computational model is thus two-dimensional. A recent numerical analysis [13] has shown that this solid-state dimension allows for a physically reliable description of intercalated TiS_2 systems (e.g. $LiTiS_2$). The stoichiometric unit employed in this work is $(NH_4)(NH_3)_3(TiS_2)_4$. This formula unit is close to the aforementioned experimental estimation of NH_4 concentration. The adopted unit cell contains 29 atoms with 97 atomic orbitals (AO's) in the valence shell.

The plot of the present paper is as follows. In Sect. 2 the structural details of our 2 D model are explained in some detail. Relevant numerical conditions of the band-structure calculations are summarized in the next part. At the beginning of Sect. 4 we give a short interpretation of important band-structure properties of bare TiS_2. Then we discuss the changes in its electronic structure upon intercalation (i.e. $(NH_4)(NH_3)_3(TiS_2)_4$). In this section we present total density of states (DOS) curves as well as their projections onto AO components. Two electronic configurations of the title system are studied. It will be shown that intercalation leads to the stabilization of a CDW-like configuration in the TiS_2 sublattice. Final remarks and conclusions are given in Section 5.

2. Two-Dimensional Model

1 T–TiS_2 crystallizes in the space-group $P\bar{3}m1$ [21]. The abbreviation 1 T symbolizes that only one layer is included in the unit cell and that the crystal system is trigonal. The experimentally determined lattice-constants are $a = 3.407$ Å and $c = 5.695$ Å, respectively. The hexagonal unit cell contains three atoms with fractional coordinates Ti(0, 0, 0), S(1/3, 2/3, 0.2501) and S(2/3, 1/3, 0.2501). On the bottom of Fig. 1 we show a projection of one TiS_2 monolayer along a direction perpendicular to the plane of the layer. The Ti atoms are located in a nearly ideal octahedral hole formed by the S centers. The structural informations

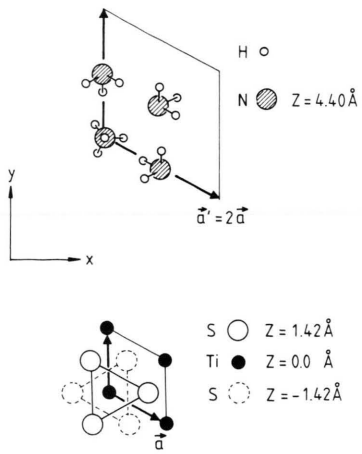

Fig. 1. Top: Projection of the intercalant layer of $(NH_4)(NH_3)_3(TiS_2)_4$ along the z-direction. Bottom: Projection of a TiS_2 layer along the z-direction. The cartesian axis used in the CO calculations are indicated. a and a' symbolize translation vectors. The N atoms of the intercalant coincide in the projection with the Ti sites of the host lattice.

available for $(NH_4)_y(NH_3)_{1-y}(TiS_2)$ are based on a X-ray powder intensity investigation [22] or have been extrapolated from ^{1}H NMR spectra [8]. The determination of an "exact" stoichiometry (i.e. magnitude of y in the above formula) was not possible via the X-ray powder study [22]. The ratio NH_4/NH_3 had been estimated in a more recent ^{1}H NMR investigation where intensity fitting-procedures lead to an approximate ratio 0.2/0.8 [8].

The X-ray analysis of ammonia TiS_2 lead to the space group R3m [22]. The translation-vectors of the hexagonal unit cell are $a = 3.427$ Å and $c = 26.55$ Å, respectively. The latter lattice-vector covers three layers. Upon intercalation with NH_3 the a and c lattice-constants of TiS_2 increase by ca. 0.6% and 55%, respectively. The N atoms of the intercalant are localized in the midplane between the host layers. The ^{1}H NMR spectra rendered possible an estimation of the spatial orientation of the NH_3 rotors; the threefold axis of NH_3 is parallel to the TiS_2 layers.

On the basis of the available structural informations on the title system we have adopted a 2D model for the CO calculations. It is defined by one TiS_2 layer; this spatial domain is supplemented by an additional 2D layer of the intercalants. In detail we have employed $(NH_4)(NH_3)_3(TiS_2)_4$ which requires the definition of a translation vector a' fulfilling $a' = 2a$. The geometry of the intercalant is symbolized on the top of Figure 1. With respect to the projection along the z direction the nitrogen positions coincide with the positions of the Ti sites of the TiS_2 host lattice. Each NH_4 unit is surrounded by six NH_3 molecules while each NH_3 has four NH_3 and two NH_4 nearest neighbours. Three of the NH_3 moieties surrounding NH_4 show an orientation where the corresponding "lone-pairs" are directed towards the NH_4 molecule (see Figure 1).

Table 1. Important interatomic distances in the 2D model $(NH_4)(NH_3)_3(TiS_2)_4$. All values in Å.

Atom pairs	Distance (Å)
Ti – S	2.43
S – S (at $+z$ and $+z$)	3.41
S – S (at $+z$ and $-z$)	3.46
S – N	3.57
N – H (NH_3)	1.03
N – H (NH_4)	1.02
Ti – N	4.40

In Table 1 we have summarized relevant interatomic distances as employed in the 2D model. The S–S separation in the 2D host lattice is too large to allow for any covalent interaction between them. The interlayer S–N distances are larger than the sum of the associated van der Waals radii (i.e. 1.80 Å for S and 1.55 Å for N, respectively [23]). Conventional covalent coupling between the two sublattices is expected to be without larger significance.

3. Computational Conditions

The employed semiempirical SCF HF CO formalism has been described in detail in recent contributions [15, 16]; the basis equations are therefore not reviewed in this context. In [16, 24] we have shown that the 2D/3D variant requires a fragmentation of the crystal into two types of spatial domains, I and II, respectively. Domain I is a sphere that has to be defined for each atomic center [24]. Within this sphere the "exact" SCF HF CO expansion is used; i.e. the interactions are treated quantum-mechanically in the adopted CO formalism. For larger interatomic separations (domain II) the interaction is expressed in terms of the conventional electrostatic Madelung approximation. In the present CO calculations we have adopted a common sphere-radius of 9 Å around each atomic site. The numerical capability of such a "boundary condition" has been analyzed in our recent investigation [24].

For the model-calculations we have adopted the two-dimensional space-group p3. The k-dependent CO equations have been solved at 9 k-points in the irreducible part of the Brillouin zone (IBZ). This grid covers an ensemble of 54 k-points in the full BZ. The k-grid in the whole BZ is required for the determination of the elements of the charge-density-bond-order matrix via Fourier transformation. The BZ as well as the irreducible part of the BZ of the employed 2D model are shown in Fig. 2. For reference we have also indicated the larger BZ associated to a single 2D TiS_2 layer.

For the numerical integration of the charge-density-bond-order matrices the plain discrete summation has been used. The occupation of the one-electron band-states is determined via suitable occupation numbers. For an analytical investigation of the accuracy of Fourier transformations in band-structure investigations we refer to [25]. The k-grid has been defined on the basis of simple geometric criteria; the corresponding sampling procedure can be identified as a special case of the large unit cell (LUC) method [26]. The SCF iterations have been controlled via an accelerated Hartree damping of the charge-density matrices [27]. An energy criterion of 10^{-4} a.u. has been established to stop the iterative process. The above conditions (i.e. sphere-radii, number of k-points, SCF criterion) require computer-times of ca. 35 min for the 2D $(NH_4)(NH_3)_3(TiS_2)_4$ system on an IBM 3090 computer working at scalar modus.

The density of states (DOS) distributions are determined by the classical histogram technique at a grid of 109 k-points in the IBZ [28]. A step-size of 0.1 eV has been used. The final curves were smoothed via Gauss-type functions with a mean-width of 0.4 eV.

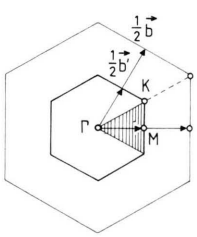

Fig. 2. Brillouin zone (BZ) (inner hexagon) and IBZ (hatched area) employed in the CO calculations of $(NH_4)(NH_3)_3(TiS_2)_4$. The outer hexagon represents the BZ of a pure TiS_2 layer (i.e. reduction of the lattice vector, extension of the BZ). b and b' are the reciprocal translation vectors corresponding to both BZ's. The symmetry points are indicated.

4. Results and Discussion

In this section we give an analysis of the band structure of $(NH_4)(NH_3)_3(TiS_2)_4$. But at first we want to discuss some important electronic-structure properties of the host lattice TiS_2. This layered material had been the subject of a large number of investigations by traditional theoretical methods in solid-state theory since the middle of the seventies [13, 29–33]. The reported band-structure calculations cover a broad spectrum of numerical methods from the classical KKR (Korringa-Kohn-Rostoker) approach [29] to the OPW (orthogonalized plane wave) [30] and APW [33] methods. In addition to the aforementioned numerical studies the system TiS_2 had been subject of different spectroscopic investigations. Band-structure parameters (i.e. widths of certain bands, gaps, etc.)

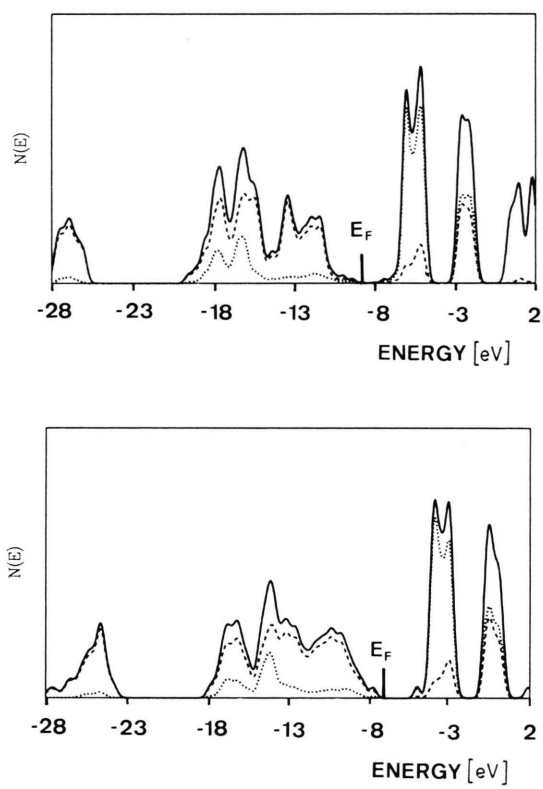

Fig. 3. Total DOS distribution (full line) of TiS_2 monolayer (top) and bulk TiS_2 (bottom) in the valence region between −28 to 2 eV. The broken lines correspond to projections onto the S 3s/3p orbitals and the dotted curves to projections onto the Ti 3d AO set. The position of the Fermi-level, E_F, is labelled in the representation.

Table 2. Experimental and calculated band structure data of TiS_2. The 3s and 3p states of S correspond to the valence band while Ti 3d stands for the conduction bands. Negative numbers for the energy gap symbolize overlapping dispersions. All energy values in eV.

Band structure parameter	LCAO [32] bulk	LAPW [13]		Present work		Experiment
		monolayer	bulk	monolayer	bulk	
S 3s – 3p gap	5.9	6.4	6.3	6.1	5.2	6–7 [34]
Net width S 3p	6.1	5.4	5.6	10.9	11.1	6–7 [35, 36]
Gap S 3p – Ti 3d (E_G)	0.7	– 0.1	– 0.5	0.8	1.6	0.17 [44]
Net width Ti 3d	3.3	4.1	4.5	6.3	6.0	4.0 [36]
$t_{2g} - e_g$ splitting	2.0	2.3	2.6	3.6	3.8	2.2 [37] 2.1 [36]

have been derived by X-ray photoelectron spectroscopy [34], He(I) and He(II) photoemission [35], apparence potential spectra [36] as well as X-ray emission and absorption measurements [37]. In the following these "experimental" quantities are compaed with numerical CO data. A priori such a comparison is not a trivial one-to-one task in Fermion systems containing transition-metal atoms. Quasi-particle (QP) corrections to the mean-field values (i.e. electronic correlations and relaxations) are often of particular importance in these materials [18, 38–41]. Green's function calculations however have shown that one-electron models are still of reliable validity for transition-metal atoms from the extreme left (i.e. Sc, Ti) or the extreme right (i.e. Cu, Zn) of the periodic system of the elements [42, 43]. The importance of virtual scattering processes is attenuated in this domain due to the limitation in the allowed particle- and hole-channels. Finally we want to mention the experimentally derived forbidden gap between the sulfur 3p valence bands and the Ti 3d conduction bands [44]. 0.17 eV have been determined by the pressure-induced band crossing at 40 Kbar. Also on the basis of angle-resolved photoemission-measurements it had been concluded that TiS_2 is a semiconductor [45].

In Fig. 3 we have shown the DOS distribution corresponding to a TiS_2 monolayer (2D model, top) and bulk TiS_2 (bottom). In the latter case a 3D CO approach has been implemented. We have displayed an energy-window from – 28 eV to 2 eV which covers the valence bands as well as the low-lying conduction bands. Comparison of the two DOS profiles shows that the band structure is properly described in terms of a 2D model (see also Table 2). The extension to a 3D approach does not introduce significant quantitative modifications. The LAPW investigation of [13] lead to the same conclusion. Figure 3 contains a decomposition of the total density of states into S 3s and 3p as well as Ti 3d contributions. The net DOS distribution is splitted into three "bundles" associated to S 3s, S 3p and Ti 3d states, respectively. The lowest maximum at ca. – 27 eV (TiS_2 monolayer) or ca. – 25 eV (bulk TiS_2) has its origin in band-states of S 3s character. The outer-valence states between ca. – 20 eV to – 9 eV (TiS_2 monolayer) and – 18 to – 7 eV (bulk TiS_2) are predominantly formed by the sulfur 3p orbitals. In the latter energetic interval metal-ligand hybridization via the Ti 3d AO's is observed. The maxima of this interaction are predicted between – 19 to – 15 eV (TiS_2 monolayer) or between – 17 to – 13 eV (bulk TiS_2). The corresponding CO microstates can be classified as Ti–S bonds. The outer-valence extension of this metal-ligand hybridization is predicted at binding energies < 10 eV.

For energies on top of the Fermi-level two maxima due to the Ti 3d states are encountered. They are separated by an energy gap and arise from the $t_{2g} - e_g$ splitting of the Ti 3d AO set in the octahedral ligand-field formed by the sulfur atoms. The center of gravity of the t_{2g}/e_g states is predicted at – 5.9/– 2.3 eV for monolayered TiS_2 and at – 4.1/– 0.3 eV for bulk TiS_2. The energetic separation (ca. 3.6 eV) is comparable in both CO descriptions. The DOS distribution as derived in the semiempirical SCF HF INDO CO formalism shows a satisfactory overall agreement with the LAPW calculations reported in [13].

In Table 2 we have summarized experimentally observed widths of characteristic band states as well as energy-gaps. These numbers are compared with the present findings and with previously published band-structure calculations [13, 32]. The numerical method adopted in [32] is a LCAO expansion containing a larger number of approximations.

The present CO formalism allows for a reliable reproduction of the 3s–3p separation of sulfur and of the width of the Ti 3d bands (i.e. octahedral t_{2g}/e_g

Table 3. Atomic net charges q_i as well as group charges in the $(NH_4)(NH_3)_3(TiS_2)_4$ CDW ground state and a "symmetry-adapted" excited state (SA) according to the SCF HF INDO CO formalism. The q_i numbers of a TiS_2 monolayer are given for comparison. The * labels symbolize averaged values.

Atom (i)	$(NH_4)(NH_3)_3(TiS_2)_4$		TiS_2 monolayer
	CDW	SA	
Ti	0.77	0.87	0.86
Ti (3 ×)	0.94	0.88	
S (+ z)	− 0.74	− 0.73	− 0.43
S (− z)	− 0.42	− 0.41	
N (NH_4)	− 0.33	− 0.33	
N (NH_3)	− 0.86	− 0.86	
H (NH_4)*	0.33	0.33	
H (NH_3)*	0.29	0.29	
Group (i)			
TiS_2*	− 0.25	− 0.25	
NH_4	0.97	0.97	
NH_3	0.01	0.01	

splitting). The total width of the S 3p bands, on the other side, is overestimated by a factor of 1.6. This shortcoming is a result of the neglect of orthogonalization effects in the employed ZDO (zero differential overlap) basis. For a physical rationalization we refer to [46]. The experimentally derived band gap E_G of TiS_2 amounts to 0.17 eV [44]. All methods summarized in Table 3 fail to reproduce E_G quantitatively. The LAPW method predicts semimetallic properties for the TiS_2 monolayer as well as for bulk TiS_2. E_G is overestimated by the two LCAO HF CO variants. This is a well-known mean-field error which is caused by the neglect of QP corrections as well as the emplomement of an unphysical potential in the virtual Fermi-sea [47]. The calculated INDO gap for a TiS_2 monolayer is close to the value reported in [32]. To summarize; the adopted semiempirical CO method allows for a reliable reproduction of experimental findings for TiS_2. Also the comparison with previous band-structure calculations shows sufficient conformity.

For $(NH_4)(NH_3)_3(TiS_2)_4$ two electronic configurations have been iterated up to SCF convergence. One is of CDW character with respect to the TiS_2 sublattice while the other is of "higher symmetry" in the latter domain, i.e. symmetry adapted (SA) solution. The SA configuration is ca. 0.56 eV (55 Kj/mol) above the CDW state. Both configurations differ in the associated Ti 3d population. The energy minimum is predicted for a conduction band formed by Ti $3d_{z^2}$ AO's. This state has been labeled as CDW; the charge densities at the two crystallographic non-equivalent Ti sites are different. The calculated net charges (Mulliken population analysis [48]) amount to 0.77 (at one Ti atom) and 0.94 (at three Ti sites). The former Ti center is located in the neighborhood of NH_4, the three (equivalent) latter Ti centers have NH_3 as nearest neighbors in the intercalant layer.

For the second SCF configuration we defined another member of the t_{2g} functions as the corresponding conduction band. The maximum CO amplitudes in this state are due to $3d_{x^2-y^2}$ and $3d_{xy}$. This 3d population converges into a mean-field solution where the TiS_2 symmetry is almost completely restored (SA configuration). The two types of Ti sites have comparable net charges, i.e. 0.87 and 0.88, respectively. The mutual deviation is less than 1.5%.

In Table 3 the atomic and fragment net charges q_i of the CDW and SA mean-field configurations of the title system are summarized. The q_i elements for pure TiS_2 are also given in the collection. The fragment net charge at NH_4 is close to + 1 (i.e. + 0.97). The NH_3 units are almost electroneutral ($q_{NH_3} = 0.01$). The numbers in Table 3 visualize the redox-character of intercalation, i.e. the nearly complete charge transfer from NH_4 to the TiS_2 sublattice. This charge transfer allows for the population of a Ti 3d band. The calculated net charges, on the other side, indicate that the surplus of electronic charge in the TiS_2 lattice is confined to the sulfur atoms. Intercalation is thus accompanied by a remarkable charge redistribution in the TiS_2 host lattice. A comparable effect has been detected in the recent LAPW calculation of $LiTiS_2$ [13]. Here the additional charge due to intercalation is seen to lie predominantly between the S and Li planes although the electron donated by Li occupies a Ti 3d band.

The net charge at S in TiS_2 is $q_s = -0.43$. As a result of intercalation the charge density at the S atoms in the neighborhood of the intercalant lattice is enhanced. For the CDW state $q_s = -0.74$ is predicted; for the SA configuration $q_s = -0.73$ is derived. The stabilization of the CDW configuration is caused partially by the enhanced electron density at S (see below). The net charges at the S centers in the $-z$ direction are comparable with the density in pure TiS_2. The CDW condensation in the mean-field ground-state leads to the following charge redistribution at the Ti sites in the TiS_2 sublattice: SA ($Ti^{0.87}$, 3 × $Ti^{0.88}$) → CDW ($Ti^{0.77}$, 3 × $Ti^{0.94}$) where

Table 4. Ti 3d AO population in the $(NH_4)(NH_3)_3(TiS_2)_4$ CDW ground-state as well as a "symmetry-adapted" excited state (SA) according to the SCF HF INDO CO approach. The occupation numbers of a TiS_2 monolayer are also given.

	$(NH_4)(NH_3)_3(TiS_2)_4$ CDW		$(NH_4)(NH_3)_3(TiS_2)_4$ SA		TiS_2
	Ti	Ti(3×)	Ti	Ti(3×)	Ti
d_{z^2}	0.80	0.24	0.19	0.20	0.21
$d_{xz} = d_{yz}$	0.63	0.74	0.77	0.77	0.77
$d_{x^2-y^2} = d_{xy}$	0.37	0.46	0.49	0.48	0.49

Table 5. AO decomposition of the conduction band of $(NH_4)(NH_3)_3(TiS_2)_4$ at the Γ point.

Atom	AO	Contribution (in %)
$Ti^{0.78}$	$3d_{z^2}$	60
	$3d_{xz}/3d_{yz}$	0
	$3d_{x^2-y^2}/3d_{xy}$	0
$Ti^{0.94}$ (3×)	$3d_{z^2}$	12
	$3d_{xz}/3d_{yz}$	18
	$3d_{x^2-y^2}/3d_{xy}$	7
S (8×)	all AO's	2
(NH_3) (3×)	all AO's	0
(NH_4)	all AO's	0

the superindex labels the corresponding atomic net charge.

In Table 4 the AO populations of the CDW and SA configurations of $(NH_4)(NH_3)_3(TiS_2)_4$ are summarized together with the numbers predicted for TiS_2. In the SA state comparable populations are derived at the crystallographically differernt Ti sites. These numbers are close to the elements calculated for the pure host lattice. A charge accumulation in $3d_{z^2}$ at those Ti sites with a net charge $q_{Ti} = 0.77$ is observed in the CDW ground-state. The corresponding 3d centers have NH_4 as next nearest neighbors (see Figure 1.). Here one has a $3d_{z^2}$ population of 0.80. At the electron deficient Ti centers ($Ti^{0.94}$) one has a $3d_{z^2}$ occupation of 0.24. The difference in the $3d_{z^2}$ population at both Ti sites in the CDW state is determined by the magnitude of the CO amplitudes in the half-filled conduction band.

The band structure of $(NH_4)(NH_3)_3(TiS_2)_4$ in the ground-state configuration is displayed in Figure 4. The calculated width of the bands is found within an interval from several tenth of an eV to ca. 4 eV. The nearly dispersionless $\varepsilon(k)$ curves at ca. -15 eV and between ca. -19 to -22 eV are due to N–H and "lone-pairs" states of the intercalant.

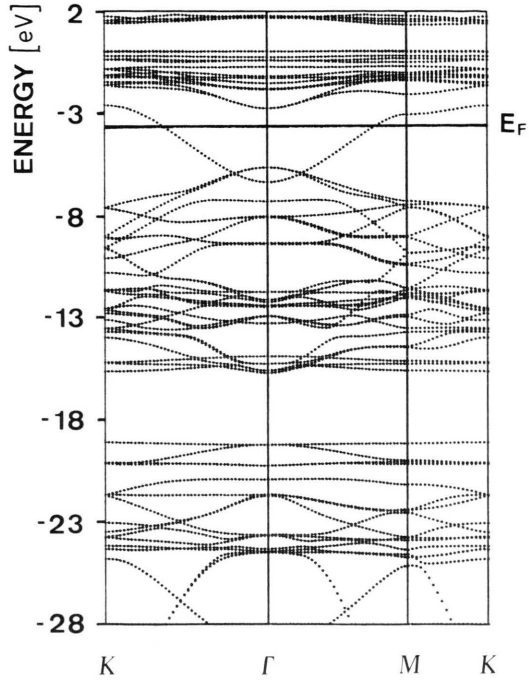

Fig. 4. Energy bands of $(NH_4)(NH_3)_3(TiS_2)_4$ in the valence region between -28 and 2 eV. The dispersion curves have been plotted along the directions of the BZ of the 2D hexagonal lattice. E_F symbolizes the Fermi-energy.

The conduction band of $(NH_4)(NH_3)_3(TiS_2)_4$ is only half-filled leading to a metallic configuration. The stoichiometric unit contains an uneven number of electrons. The charge transfer from the intercalant to the host-lattice (via a redox-process) is therefore accompanied by a semiconductor-to-metal transition in the intercalation system. This metallic character is in line with experimental findings [3]. The calculated width of the conduction band is 3.8 eV. The bottom of the band is predicted at -6.4 eV (Γ point) and the top at -2.6 eV (K point). The Fermi-energy is calculated at -3.7 eV. The analytic structure of the conduction band is close to an idealized "tight-binding" relation.

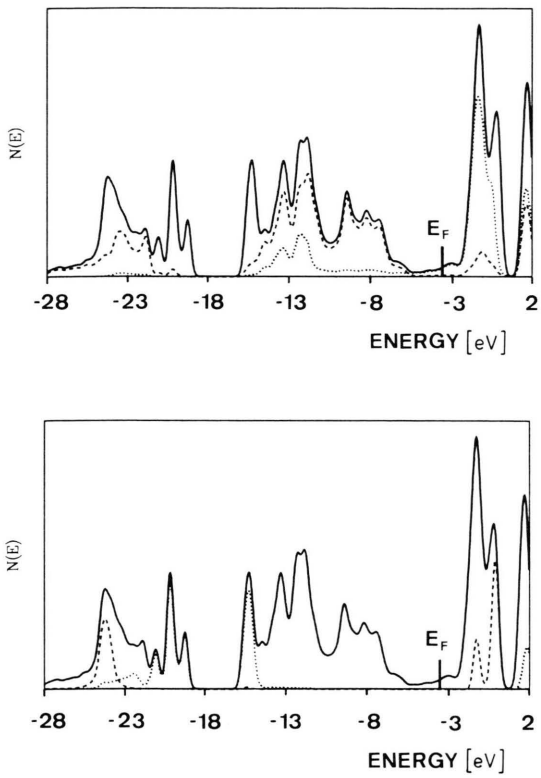

Fig. 5. Total DOS (full line in both diagrams) of $(NH_4)(NH_3)_3(TiS_2)_4$ in the valence region between -28 and 2 eV. In the lower representation we have given the projections onto the NH_4 states (broken curve) as well as onto the NH_3 states (dotted curve). In the upper DOS distribution projections onto sulfur 3s/3p (broken curve) and Ti 3d (dotted curve) are given. The position of the Fermi-energy is indicated in both diagrams.

In Tab. 5 we have summarized the AO amplitudes of the CO microstates at the Γ point. We determined a Ti contribution of 98%. The occupation of these states is a consequence of the aforementioned redox-process upon intercalation. The leading AO amplitude corresponds to the $3d_{z^2}$ function of the $Ti^{0.77}$ site. The corresponding Ti 3d population is responsible for the formation of a CDW state. The destabilization of the conduction band along $\Gamma \rightarrow K$ (and also along $\Gamma \rightarrow M$) is a consequence of an antibonding metal-ligand interaction. The resulting sulfur admixtures at Γ amount to 2% while at K they increase to 10%. Admixtures from the intercalant are not encountered. A 0.7 eV overlap between the Ti 3d states (conduction band) and the S 3p levels (outer-valence region) is observed. In the pure TiS_2 host both are separated by 0.8 eV (2D model).

The DOS distribution of $(NH_4)(NH_3)_3(TiS_2)_4$ is shown in Fig. 5. The net DOS curve has been decomposed into AO projections associated to the NH_4 and NH_3 units (lower diagram) as well as to the S 3s/3p and Ti 3d AO's (upper diagram). A comparison with Fig. 3 (top, i.e. DOS of a TiS_2 monolayer) shows the formation of new states in the DOS curve of the title system which are associated to the intercalant. The energy gap between the S 3s and 3p states in the host lattice (gap: 6.1 eV, see Table 2) is partially filled by states confined to the NH_3 molecules. The "reduced" energy gap in the title system amounts to ca. 2.5 eV.

The two peak-maxima in Fig. 5 at ca. -15.5 eV and -20 eV, respectively, correspond to "lone-pair" states as well as N – H functions of ammonia. Hybridization of these states with CO functions associated to the host sublattice is without larger significance. The one-electron energies of NH_4 are predicted at ca. -24 eV, i.e. 4 eV below the lowest filled valence states of NH_3. This energetic separation is a consequence of the different charge densities at both types of N atoms. The corresponding net charge, q_i, in the NH_3 unit is -0.86 while -0.33 is derived for the nitrogen-site in NH_4. Intercalation is not accompanied by remarkable changes in the DOS distribution associated to S 3p. Also the Ti 3d states involved in the Ti – S bonds are only little modified. The most important change is the suppression of the energy gap between the S 3p and Ti 3d functions.

In the following we will explain the electrostatic origin favouring the CDW configuration. In recent contributions one of the present authors has analyzed the stabilization of mixed valence states in 1 D materials [49–51] and the condensation of CDW's in materials with interactions that are higher than 1 D [52, 53]. The formation of symmetry broken (SB) or CDW configurations is here always favoured by the classical Coulomb energy. It should be mentioned that it was not possible to stabilize a SA-type mean-field solution for an electronic configuration where the conduction band is formed by $3d_{z^2}$. On the other side no stable CDW-type solution was feasible for the second Ti 3d allocation in the conduction band. The $3d_{z^2}$ occupation leads always to the CDW condensation while the $3d_{x^2-y^2}/3d_{xy}$ allocation is accompanied by a restoration of the site symmetry in the TiS_2 sublattice.

The INDO approximation of the present CO formalism renders possible a decomposition of the total energy of the periodic solid into transparent terms of physical significance. The theoretical background of

Table 6. Energy fragmentation for the two mean-field states of $(NH_4)(NH_3)_3(TiS_2)_4$ according to the semiempirical SCF HF CO approach. The abbreviations have been explained in the text. The corresponding numbers are energy differences between the CDW and SA state. The SA elements have been used as internal standard. Negative parameters correspond to a stabilization of the CDW configuration. All values in eV.

	Relative energy
TOTAL	− 0.56
INTERCELL	+ 0.66
INTRACELL	− 1.23
one-center	+ 0.14
two-center	− 1.37
hopping	− 0.01
Coulomb	− 1.26
exchange	− 0.10

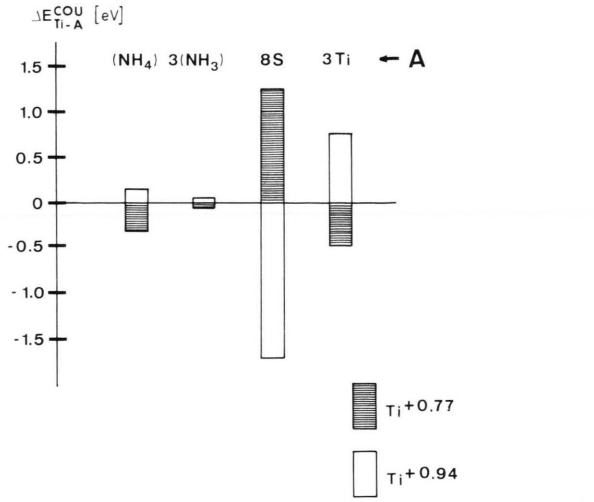

Fig. 6. Relative Coulomb energies between a Ti site and other atomic centers A in the reference cell of $(NH_4)(NH_3)_3(TiS_2)_4$. The index A is used to abbreviate different groups of atoms in the cell. The relevant classical electrostatic energies are given for both types of Ti atoms. The elements for a SA state are used as internal standard. Relative energies < 0 symbolize a stabilization of the CDW configuration.

this partitioning-technique has been given in [15]. The results of an energy fragmentation for the CDW and SA configurations of $(NH_4)(NH_3)_3(TiS_2)_4$ are collected in Table 6. The considered energy differences are subsequently defined. The SA solution has been employed as internal standard. Numbers smaller than 0 indicate always the stabilization of the CDW state: difference in the total energy (TOTAL), as well as intercell (INTER) and intracell (INTRA) energy. The INTRA parameter of TOTAL is subdivided into one- and two-center contributions. The former elements are purely atomic quantities while the latter correspond to the sum of all diatomic interaction energies. The two-center part is furthermore fragmented into the kinetic hopping term, the classical Coulomb energy as well as the nonclassical exchange contributions which are a result of the determinantal character of the HF CO wave function.

According to the data of Tab. 6 the CDW stabilization is caused by the two-center Coulomb elements in the reference cell. In Fig. 6 we have displayed the response in the "two-center" Coulomb terms upon CDW condensation. In detail we have considered the classical Coulomb-energy E^{COU}_{Ti-A} between a Ti site and ensembles of other atoms or molecular fragments A. The index A stands for the remaining three Ti sites per cell, the eight sulfur atoms, the three (NH_3) moieties as well as NH_4. The energy-elements of the SA configuration have been adopted as internal standard.

The CDW condensation is controlled by the balance between attractive and repulsive Coulomb interactions. A stabilization due to changes in the net charge at one type of the Ti sites is always accompanied by an energetic destabilization via the second type of 3d centers. The results displayed in Fig. 6 indicate that the interplay between attractive and repulsive Coulomb terms is largely determined by two elements favouring CDW condensation. The first is the $Ti - NH_4$ coupling; i.e. the repulsive Coulomb term is attenuated due to the charge accumulation at $Ti^{0.77}$. The second term favouring the CDW configuration corresponds to the Ti – S pairs. This coupling-energy is largest for the $Ti^{0.94}$ sites. The $Ti - NH_3$ interaction is without larger significance for the net energy-balance. There is only one element which counteracts the CDW condensation, i.e. the mutual Ti – Ti interaction.

5. Final Remarks and Conclusions

The band structure of the intercalation system $(NH_4)(NH_3)_3(TiS_2)_4$ has been studied by a semiempirical SCF HF CO formalism. The stoichiometry and the spatial arrangement of the molecular subunits have been selected on the basis of available experimental informations (e.g. ^1H NMR spectra). The uneven number of electrons per stoichiometric unit leads to a metallic configuration; the highest occupied states are of Ti 3d character. High conductivities with metallic temperature-dependence are conventionally

observed in intercalation compounds formed by TX_2 host lattices, where T is a d^0 transition-metal atom. The CO calculations of the title system have shown that the electron density at the transition-metal sites is comparable with the density at Ti of the pure TiS_2 host although new Ti 3d states at the Fermi-level are predicted for $(NH_4)(NH_3)_3(TiS_2)_4$. The net intercalant to host lattice charge transfer is prevailingly confined to the sulfur atoms. The electronic reorganization concerning Ti is of an intraatomic-type.

The interaction between the host lattice and the intercalant is of Coulomb character; covalent contributions are only of minor significance. This Coulomb potential leads to a CDW-like configuration for the TiS_2 sublattice in the electronic ground-state. The associated conduction band is of Ti $3d_{z^2}$ character. The adaptation of a conduction band formed by Ti $3d_{x^2-y^2}/3d_{xy}$ allows for the identification of a second mean-field state 0.56 eV (55 Kj/mol) above the ground-state. This configuration is of higher symmetry in the TiS_2 sublattice, i.e. the charge distribution at all Ti sites is roughly comparable. The CDW ground-state, on the other side, can be characterized as mixed-valence configuration.

We have also discussed some band-structure properties of pure TiS_2. The present CO data have been compared with available experimental data and numerical results of other band-structure investigations. These comparisons indicate the reliable accuracy of the adopted tight-binding description.

Acknowledgements

We are grateful to Prof. Dr. Alarich Weiss for his continuous interest in this work. This investigation has been supported by the Deutsche Forschungsgemeinschaft.

[1] J. A. Wilson and A. D. Yoffe, Adv. Phys. **18,** 193 (1969).
[2] V. Grasso (ed.), Electronic Structure and Electronic Transitions in Layered Materials, D. Reidel, Dordrecht 1986.
[3] R. H. Friend and A. D. Yoffe, Adv. Phys. **36,** 1 (1987).
[4] P. W. Williams, in: Crystallography and Crystal Chemistry of Materials with Layered Structures, F. Levy (ed.), D. Reidel, Dordrecht 1976.
[5] R. Schöllhorn, Physica **99 B,** 89 (1980).
[6] F. R. Gamble, J. H. Osiecki, and F. J. DiSalvo, J. Chem. Phys. **55,** 3525 (1971).
[7] R. Schöllhorn and H. D. Zagefka, Angew. Chem. **89,** 193 (1977); Angew. Chem. Int. Ed. Engl. **16,** 199 (1977).
[8] E. Wein, W. Müller-Warmuth, and R. Schöllhorn, Sol. State Ionics **22,** 231 (1987).
[9] R. Schöllhorn, H. D. Zagefka, T. Butz, and A. Lerf, Mat. Res. Bull. **14,** 369 (1979).
[10] C. Y. Fong and M. Schlüter, in: Electrons and Phonons in Layered Crystal Structures, T. J. Wieting and M. Schlüter (eds.) D. Reidel, Dordrecht 1979.
[11] E. Doni and N. Girlanda, in: Electronic Structure and Electronic Transitions in Layered Materials, V. Grasso (ed.), D. Reidel, Dordrecht 1986, page 1.
[12] J. V. McCanny, J. Phys. C: Solid State Phys. **12,** 3263 (1979).
[13] C. Umrigar, D. E. Ellis, D. Wang, H. Krakauer, and M. Posternak, Phys. Rev. **B 26,** 4935 (1982).
[14] T. Yamasaki, N. Suzuki, and K. Motizuki, J. Phys. C: Solid State Phys. **20,** 395 (1987).
[15] M. C. Böhm, Theor. Chim. Acta **62,** 351 (1983).
[16] R. Ramírez and M. C. Böhm, Int. J. Quantum Chem., in press.
[17] M. C. Böhm, R. Ramírez, and A. M. Oleś, Ber. Bunsenges. Phys. Chem. **91,** 717 (1987).
[18] M. C. Böhm, One-Dimensional Organometallic Materials, Lecture Notes in Chemistry, Vol. **45,** Springer-Verlag, Berlin 1987 and references cited therein.
[19] R. Ramírez, R. Nesper, H. G. von Schnering, and M. C. Böhm. Z. Naturforsch. **42 a,** 670 (1987).
[20] R. Ramírez and M. C. Böhm, Int. J. Quantum Chem. in press.
[21] A. H. Thompson, F. R. Gamble, and R. Symon, Mat. Res. Bull. **10,** 915 (1975).
[22] R. R. Chianelli, J. C. Scanlon, M. S. Whittingham, and F. R. Gamble, Inorg. Chem. **14,** 1691 (1975).
[23] A. Bondi, J. Phys. Chem. **68,** 44 (1964).
[24] R. Ramírez and M. C. Böhm, phys. stat. sol. b **135,** 661 (1986).
[25] F. Pfirsch and M. C. Böhm, Chem. Phys. **98,** 89 (1985).
[26] R. Ramírez and M. C. Böhm, Int. J. Quantum Chem. **30,** 391 (1986).
[27] D. R. Hartree, The Calculation of Atomic Structure, Wiley Interscience, New York 1957.
[28] J. Brust, in: Methods in Computational Physics, Vol. **8,** B. Alder, S. Fernbach, and M. Rothenberg (eds.) Plenum Press, New York 1968.
[29] H. W. Myron and A. J. Freeman, Phys. Rev. **B 9,** 906 (1977).
[30] P. Krusius, J. von Boehm, and H. Isomaki, J. Phys. C: Solid State Phys. **8,** 3788 (1975).
[31] A. Zunger and A. J. Freeman, Phys. Rev. **B 16,** 906 (1977).
[32] D. W. Bullett, J. Phys. C: Solid State Phys. **11,** 4501 (1978).
[33] G. A. Benesh, A. M. Woolley, and C. Umrigar, J. Phys. C: Solid State Phys. **18,** 1595 (1985).
[34] G. K. Wertheim, F. J. DiSalvo, and D. N. E. Buchanan, Solid State Commun. **13,** 1225 (1973).
[35] P. M. Williams and F. R. Shepherd, J. Phys. C: Solid State Phys. **6,** L 36 (1973); ibid. **7,** 4416 (1974).
[36] C. Webb and P. M. Williams, Phys. Rev. **B 11,** 2082 (1975).
[37] D. W. Fischer, Phys. Rev. **B 8,** 3576 (1973).
[38] A. B. Kunz and G. T. Surratt, Solid State Commun. **25,** 9 (1978).
[39] A. Bakshai, L. M. Holaday, D. Eknayan, and N. E. Brener, Phys. Rev. **B 29,** 6932 (1984).
[40] M. C. Böhm, phys. stat. sol. b **127,** 209 (1985).

[41] M. C. Böhm, Int. J. Quantum Chem. **27,** 323 (1985).
[42] M. C. Böhm, J. Chem. Phys. **78,** 7044 (1983).
[43] M. C. Böhm, J. Phys. B: At. Mol. Phys. **17,** 3101 (1984).
[44] P. C. Klipstein and R. H. Friend, J. Phys. C: Solid State Phys. **17,** 2713 (1984).
[45] C. H. Chen, W. Fabian, F. C. Brown, K. C. Woo, B. Davies, B. Delong, and A. H. Thompson, Phys. Rev. **B 21,** 615 (1980).
[46] P. R. Underhill and J. A. D. Matthew, J. Phys. C: Solid State Phys. **13,** L 791 (1980).
[47] M. C. Böhm, Solid State Commun. **46,** 709 (1983).
[48] R. S. Mulliken, J. Chem. Phys. **23,** 1833 (1955).
[49] M. C. Böhm, J. Chem. Phys. **81,** 855 (1984).
[50] M. C. Böhm, Z. Naturforsch. **39 a,** 807 (1984).
[51] M. C. Böhm, Z. Physik B: Condensed Matter **56,** 99 (1984).
[52] M. C. Böhm, phys. stat. sol. (b) **121,** 255 (1984).
[53] M. C. Böhm, Physica **124 B,** 327 (1984).